Chapter 7

Reactive Uptake of Ammonia by Biogenic and Anthropogenic Organic Aerosols

Julia Montoya-Aguilera,[1] Mallory L. Hinks,[1] Paige K. Aiona,[1] Lisa M. Wingen,[1] Jeremy R. Horne,[2] Shupeng Zhu,[2] Donald Dabdub,[2] Alexander Laskin,[3] Julia Laskin,[3] Peng Lin,[3] and Sergey A. Nizkorodov[1,*]

[1]Department of Chemistry, University of California, Irvine, California 92697, United States
[2]Department of Mechanical and Aerospace Engineering, University of California, Irvine, California 92697, United States
[3]Department of Chemistry, Purdue University, West Lafayette, Indiana 47907, United States
[*]E-mail: nizkorod@uci.edu

Secondary organic aerosol (SOA) produced by photooxidation of biogenic and anthropogenic volatile organic compounds (VOCs) represent a large fraction of fine atmospheric particulate matter ($PM_{2.5}$). The chemical composition of SOA particles is continuously changing as a result of various chemical and physical aging processes. One of the recently discovered aging processes, observed in both laboratory and field experiments, is the reactive uptake of ammonia by carbonyl species in SOA, leading to the formation of nitrogen-containing organic compounds (NOC). These NOC have attracted a lot of attention because of their propensity to absorb visible radiation and increase the amount of solar energy trapped in the atmosphere. Another potentially important, but poorly explored, consequence of NOC formation is that these compounds are less efficient than ammonia at neutralizing acids in particles. This paper summarizes existing experimental evidence for the reactive uptake of ammonia by SOA particles and describes our recent efforts to model the effect of this complicated process on air quality at the regional and continental scale. The modeling results predict that the reactive

uptake of ammonia by SOA particles can significantly reduce the concentration of gas-phase ammonia, thereby indirectly affecting particle acidity as well as the amount of ammonium sulfate and ammonium nitrate in PM$_{2.5}$. Since emissions of ammonia to the atmosphere are expected to increase due to the growing agricultural needs of the human population, these findings have important implications for future air pollution control strategies.

Sources and Sinks of Atmospheric Ammonia

Ammonia (NH$_3$) is an important atmospheric trace gas emitted into the atmosphere by a number of natural and anthropogenic sources including soils, oceans, animal husbandry, fertilizer use, automobiles, and biomass burning (*1–3*). The largest source of ammonia is agriculture, which accounts for roughly half of the global ammonia emissions, including those from animal waste and fertilizer use. Remote observations of ammonia from space have revealed hot spots of ammonia concentrations in areas known for intense agricultural activities such as the Central Valley of California, North China Plain, Indo-Gangetic Plain, and Fergana Valley in Uzbekistan (*4*).
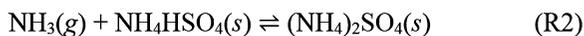
Depending on the location, the sources of ammonia can deviate strongly from the global average. For example, in the South Coast Air Basin of California (SoCAB), the amount of ammonia emitted by automobiles is on the same order of magnitude as that from agricultural sources (*5*). This results in a more uniform distribution of ammonia throughout the SoCAB, but hot spots around agricultural areas are still present, for example in Chino, a major center for dairy farming.

Ammonia is a highly water-soluble molecule, therefore it is primarily lost by deposition on water-containing particles and aquatic surfaces (*6*). Oxidation of gaseous ammonia by OH is relatively slow, but the chemistry of the resulting NH$_2$ radical contributes to the sources of N$_2$O (*2*). Atmospheric NH$_3$ in the gas-phase and NH$_4^+$ in the condensed-phase are often considered together as NH$_x$ in literature dealing with the global nitrogen cycle. Human activities not only dominate ammonia emissions, but also determine where reactive nitrogen is deposited, with terrestrial ecosystems now receiving relatively more NH$_x$ than marine ecosystems (*7*).

Chemistry of Ammonia in Particulate Matter

Ammonia is the most important atmospheric basic species capable of neutralizing inorganic acids, such as sulfuric acid and nitric acid, commonly found in polluted air. The resulting inorganic ammonium salts have low volatility and condense as solids into fine particulate matter (PM$_{2.5}$, particles with sizes below 2.5 μm, which more easily penetrate the respiratory tract).

$$NH_3(g) + H_2SO_4(g) \rightleftharpoons NH_4HSO_4(s) \tag{R1}$$

$$NH_3(g) + NH_4HSO_4(s) \rightleftharpoons (NH_4)_2SO_4(s) \qquad \text{(R2)}$$

$$NH_3(g) + HNO_3(g) \rightleftharpoons NH_4NO_3(s) \qquad \text{(R3)}$$

For example, almost half of the PM$_{2.5}$ mass in the SoCAB is due to ammonium sulfate and ammonium nitrate (8, 9). The equilibria R1-R3 are simplified representations of the actual reactions, which occur in multiple phases and involve water. In particles containing liquid water, ammonia and acids are scavenged by droplets resulting in coupled aqueous equilibria involving NH_4^+(aq), HSO_4^-(aq), SO_4^{2-}(aq), and NO_3^-(aq). We note that complete neutralization of sulfuric acid in (R2) requires unrealistically high concentrations of ammonia (10, 11), so ambient particles remain acidic under typical atmospheric conditions.

In addition to the reasonably well constrained inorganic acid-base chemistry of ammonia, recent experiments have shown that ammonia can react with certain organic compounds in primary organic aerosol (POA, particles containing organic compounds directly emitted into the atmosphere by various sources) and in secondary organic aerosol (SOA, a collection of particle-phase organic compounds formed by photooxidation of volatile organic compounds (VOCs)). The general mechanism involves the reaction of ammonia with carbonyls within the organic particles to produce relatively unstable imines and amines, which may be stabilized by intramolecular cyclization into heteroaromatic products based on imidazole, pyrrole, indole, etc. These reactions change not only the chemical composition of organic particles but also their physical properties. For example, they can produce chromophoric organic compounds capable of absorbing visible radiation, known as brown carbon (BrC) (12). Additionally, uptake of ammonia modifies particle viscosity and condensed-phase diffusivity of SOA components (13–15).

Early interest in this chemistry can be traced to a serendipitous observation by Mang et al. (2008) that SOA samples prepared by ozonolysis of d-limonene (LIM/O$_3$ SOA) reproducibly turned brown when they were exposed to ambient air for a few days (16). Figure 1 reproduces the absorption spectrum published by Mang et al. (2008) of LIM/O$_3$ SOA particles collected on an optical window as a function of storage time in open air. The SOA material became more light-absorbing throughout the visible spectrum, with the largest change appearing in the form of a characteristic absorption band at 510 nm.

The reason for the browning of LIM/O$_3$ SOA material was not known until Bones et al. (2010) demonstrated that this process involves a complex reaction between ammonium/ammonia and carbonyl compounds in LIM/O$_3$ SOA (17). There must have been enough ammonia emitted by the laboratory personnel to cause the LIM/O$_3$ SOA material to slowly change color over time in the original Mang et al. (2008) experiments. Follow up experiments have shown that browning chemistry is not limited to LIM/O$_3$ SOA; similar browning processes were observed in a broad range of other types of biogenic and anthropogenic SOA (18). The mechanism of the reaction was examined by high-resolution mass spectrometry (HRMS), which found that highly-conjugated light-absorbing nitrogen-containing organic compounds (NOC) were responsible for the brown color of the aged SOA material (19–23).
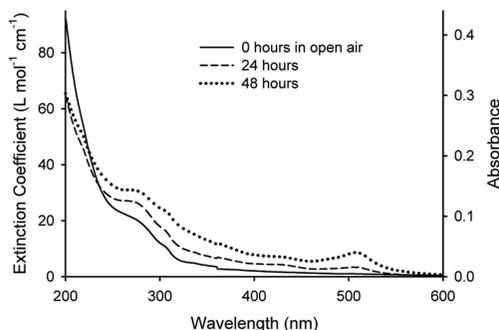
Figure 1. Absorption spectra of LIM/O₃ SOA material collected on a CaF₂ window as a function of storage time in open room air in darkness. The observed changes in the absorption profile were accompanied by a visible transition of the material from colorless to red-brown. The figure is reproduced with permission from ref. (16). Copyright 2017 American Chemical Society.

Even when SOA particles did not visibly change their color upon exposure to ammonia, NOC were still produced in the particles. For example, α-pinene ozonolysis SOA (APIN/O₃ SOA) remained colorless, meanwhile LIM/O₃ SOA browned after exposure to ammonia, but both samples had a number of relatively similar NOC products observed by HRMS methods (*20*). The stark contrast in the browning behavior of APIN/O₃ and LIM/O₃ SOA suggested that chromophoric NOC are highly conjugated oligomers of Schiff bases present at relatively low concentrations. The formation of these types of chromophoric compounds in APIN/O₃ SOA is hindered by the structural rigidity of the α-pinene oxidation products, compared to the much more flexible products of d-limonene oxidation (*20*).

Another important browning reaction identified in laboratory experiments is the aqueous reaction of 1,2-dicarbonyls, such as glyoxal and methyl glyoxal, with ammonia, amines, and amino acids (*24–54*). These reactions are capable of chemically trapping volatile glyoxal and methyl glyoxal in the form of oligomerized, light-absorbing products, thus providing an efficient pathway to secondary BrC formation. Their formation proceeds through imidazole by a mechanism described by Heinrich Debus in 1858 (*55*). The imidazole compounds attributed to this reaction have now been observed in ambient particles (*56, 57*) and shown to act as efficient photosensitizers (*40, 48, 58–60*). These types of compounds are believed to build up in aerosol particles at night but are quickly photolyzed during the day (*36, 45, 48, 50, 51*). The photolysis experiments cited here have been carried out only in the aqueous phase. The photochemical stability of these imidazole compounds in dry aerosol particles has not been studied yet.

The browning reactions between ammonia and 1,2-dicarbonyls are closely related to the Maillard chemistry responsible for the browning of foods during cooking driven by reactions of amino acids and reducing sugars (*49, 61–64*). Our current understanding of the SOA browning mechanism is that this reaction also requires a dicarbonyl species that can cyclize into a stable heterocyclic aromatic

compound in a reaction with ammonia (*19, 65*). For example, Figure 2 shows the mechanism of the reaction of 4-oxopentanal, the simplest atmospherically relevant 1,4-dicarbonyl, with ammonia. The reaction involves a carbonyl-imine conversion of the aldehyde group, followed by intramolecular cyclization to form 2-methyl pyrrole (*19*). The amine intermediate is not very stable, but the cyclization drives the reaction downhill in free energy. The pyrrole can continue reacting with additional 4-oxopentanal molecules and ammonia to produce larger products capable of absorbing visible light. Similar chemical processes are expected to occur during reactions of ammonia with ketoaldehydes derived from oxidation of monoterpenes, for example in the case of browning of ketolimononaldehyde (*21*).
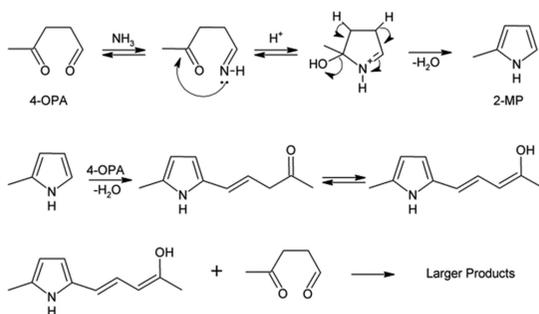

Figure 2. (Top) 4-oxopentanal reacts with NH_3 to form 2-methyl pyrrole, an intermediate to the production of BrC chromophores. (Bottom) 2-methyl pyrrole further reacts with 4-oxopentanal to form dimer products. A series of such reactions can produce larger, conjugated products potentially capable of absorbing visible light. The figure is reproduced with permission from ref. (19). Copyright 2017 American Chemical Society.

The majority of previous studies have described mechanistic aspects of reactions between ammonia and SOA compounds, but only a few studies have examined the kinetics of reactive uptake of ammonia by SOA particles. The most important study for this discussion is that by Liu et al. (2015) who reported uptake coefficients for ammonia onto $APIN/O_3$ SOA and m-xylene photooxidation SOA particles (XYL/OH SOA) (*66*). The uptake coefficients were obtained by measuring the rate of appearance of NOC in particles with a time-of-flight aerosol mass spectrometer (ToF-AMS) after their exposure to a pulse of gaseous ammonia. All experiments were carried out at a relative humidity (RH) of 50% (the critical role of RH in reactive uptake of ammonia is discussed below). Figure 3 reproduces a key result from that study, in which the uptake resulting in NOC formation is quantified for $APIN/O_3$ SOA grown on acidic or neutral seed particles. The observed initial uptake coefficients were quite high, on the order of $\gamma = 10^{-2}$ to 10^{-3} in both $APIN/O_3$ SOA and XYL/OH SOA, but after several hours of reaction they decreased to $\gamma \sim 10^{-5}$. The uptake coefficient was higher for particles that were acidified, with signals from both NOC and ammonium ion increasing with particle acidity. The weight fraction of NOC after the exposure

was estimated as ~10 wt% for APIN/O_3 SOA and ~30 wt% for XYL/OH SOA. This suggested that a significant fraction of nitrogen could enter the particles not in the traditional form of organic and inorganic salts of ammonia, but also in the form of NOC. The decreasing uptake coefficients with time suggest a kinetic limitation to this uptake.
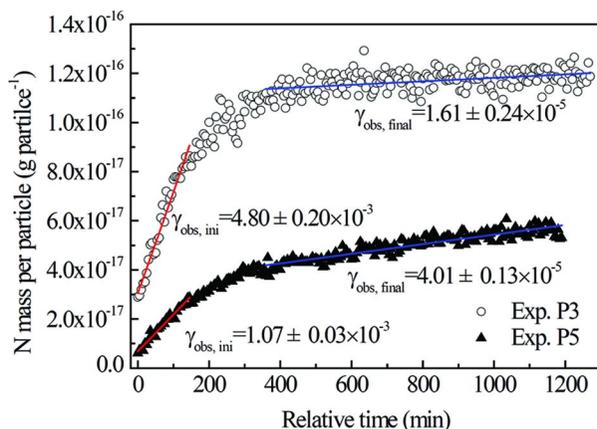

Figure 3. Reactive uptake coefficients for ammonia onto APIN/O_3 SOA particles at 50% RH. Experiment P3 corresponds to SOA produced using seed particles acidified with sulfuric acid, whereas experiment P5 corresponds to SOA produces using neutral seed particles. The figure is reproduced with permission from authors of Ref. (66). Copyright 2015 under creative commons attribution license.

A recent series of laboratory experiments highlighted the important role that RH can play in the reactive uptake of ammonia by SOA particles (*13–15*). Liu et al. (2018) examined the interactions between ammonia and SOA particles prepared by low-NO_x photooxidation of toluene (TOL/OH SOA) by tracing characteristic $C_xH_yN_z^+$ ions from ToF-AMS measurements that can only be produced by NOC (*15*). Figure 4 shows that the ratio of NOC mass concentration to total organic mass concentration is low under dry conditions, but increases at higher RH. This result was attributed to the high viscosity and slow molecular diffusion in TOL/OH SOA particles under dry conditions (*67*). The model accounting for the slow diffusion showed that the reaction was limited by the low diffusivity of the large organic molecules from the interior region of the particle to the surface. The diffusivity limitations no longer applied at higher RH because of the known ability of humid air to make organic materials less viscous (*68*). The observed transition from the lack of reactivity to full reactivity between 30-60 % RH is consistent with the independent result of Ye et al. (2016), who observed that the mass-transfer limitation for gas-particle partitioning in TOL/OH SOA was removed at RH above 40% (*69*). In another set of experiments (*14*), APIN/O_3 SOA particles exposed to ammonia under dry conditions developed a semi-solid coating on the surface (consisting of ammonium carboxylates) which prevented further reaction and also slowed down the particle coagulation. From these observations, we conclude that

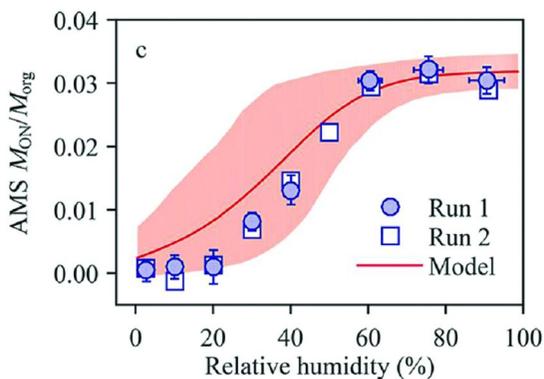ammonia + SOA particle reactions leading to NOC are not efficient under dry conditions.

Figure 4. The ratio of NOC mass concentration to total organic mass concentration at different RH values. The reaction is suppressed at low RH by the high viscosity of TOL/OH SOA particles. The figure is reproduced with permission from ref. (15). Copyright 2018 American Chemical Society.

We carried out related experiments in our laboratory with LIM/O$_3$ SOA, as well as SOA particles prepared by low-NO$_x$ and high-NO$_x$ photooxidation of toluene (TOL/OH SOA and TOL/OH/NO$_x$ SOA), n-hexadecane (HEX/OH SOA and HEX/OH/NO$_x$ SOA), and d-limonene (LIM/OH SOA and LIM/OH/NO$_x$ SOA) in a 5 m^3 Teflon chamber. Details of the experiments are provided in the Ph.D. dissertation of Dr. Mallory L. Hinks (*70*). All experiments were carried out at 50% RH to prevent the mass-transfer limitations described above. While oxidation of anthropogenic toluene and n-hexadecane usually happens under high-NO$_x$ conditions in ambient air, the control experiments carried out under low NO$_x$ conditions were helpful in distinguishing contributions to particulate nitrogen from ammonium nitrate, NOC produced during the photooxidation, and NOC produced by the subsequent reactive uptake of ammonia. Both high-NO$_x$ and low-NO$_x$ conditions are relevant for biogenic d-limonene, because it is found in both urban and remote environments.

Figure 5 shows how the mass concentration of TOL, HEX, and LIM SOA particles responds to a 50 ppb pulse of ammonia. In all cases, the low NO$_x$ experiments showed no significant change in particle mass loading, whereas there was a clear increase in the particle mass loading in high-NO$_x$ experiments. This increase in particle mass concentration in the high-NO$_x$ experiments was accompanied by an increase in the average particle size, and it can be attributed to the reaction (R3) between ammonia and nitric acid, where the latter is produced by the normal oxidation of NO$_x$ in the chamber. The lack of effect of ammonia on the particle mass concentration and size in the low NO$_x$ experiments can be best understood by examining the reaction shown at the top of Figure 2. The uptake of ammonia is expected to convert carbonyls into imines and aromatic NOC by the loss of one or several water molecules. Since the molecular weight of

ammonia reactant and water product is about the same, we do not expect a large change in the molecular weight of the organic reactants when they are converted to NOC. Indeed, the experiments by Liu et al. (2015) described above also found no significant change in the SOA particle mass concentration after exposure to ammonia (*66*).
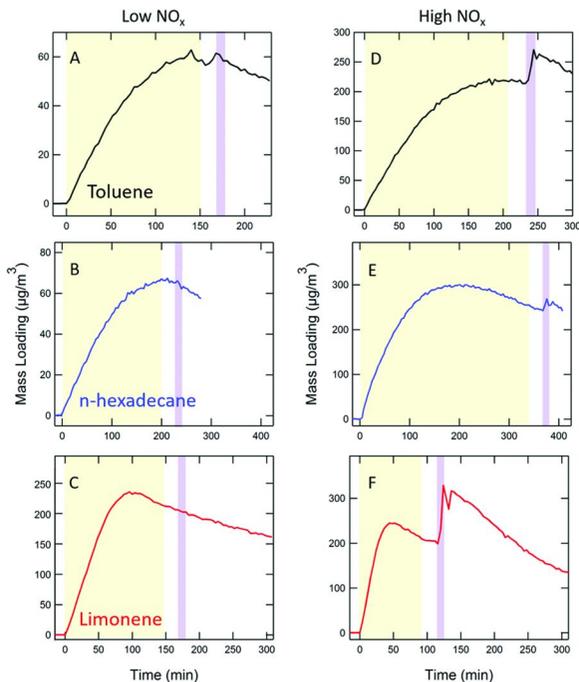

Figure 5. Mass concentration of particles during low-NO$_x$ (left panels) and high-NO$_x$ (right panels) photooxidation of toluene (a and d), hexadecane (b and e) and d-limonene (c and f). The yellow area indicates the time during which the chamber lamps were on. The purple area indicates the time during which a 50 ppb pulse of ammonia was introduced to the chamber. Reproduced with permission from the Ph.D. dissertation by Mallory Hinks (70). Copyright 2017 under creative commons attribution license.

Even though there is no apparent particle size change in low-NO$_x$ experiments, the formation of NOC could be confirmed from the increase in the peaks attributable to C$_x$H$_y$N$_z^+$ ions in ToF-AMS mass spectra (Figure 6). The specific fragments that were observed to increase were CHN$^+$, C$_2$H$_3$N$^+$, C$_2$H$_4$N$^+$, and C$_3$H$_8$N$^+$. The lack of any effect on the NH family of fragments (NH$^+$, NH$_2^+$, NH$_3^+$, and NH$_4^+$) and the NO family of fragments (NO$^+$, NO$_2^+$, and NO$_3^+$) confirms that no ammonium nitrate impurity or ammonium carboxylates were produced during exposure of LIM/O$_3$ to ammonia. Since under low-NO$_x$ conditions, the only possible source of nitrogen in the particles is the SOA + NH$_3$

reaction, this observation supports the assumption that ammonia is being taken up by the SOA particles and reacts with carbonyls in the particles forming NOC.
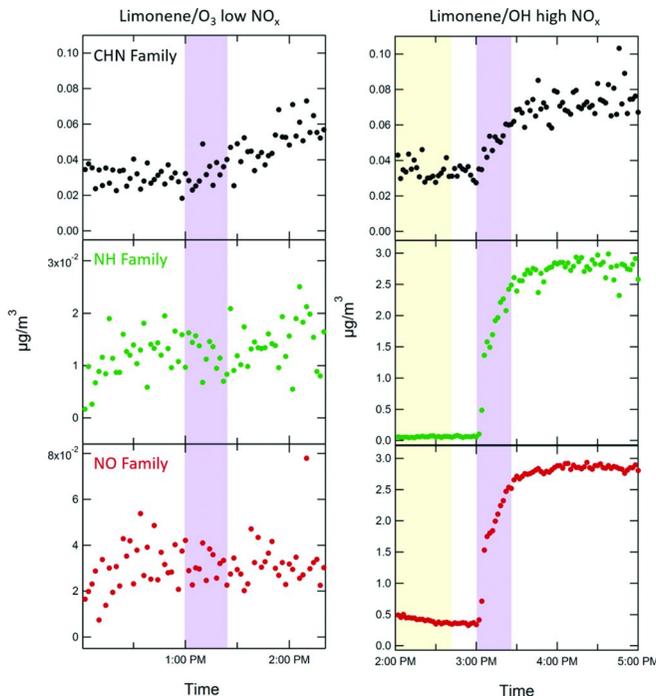

Figure 6. ToF-AMS data for LIM/O₃ SOA (left panels) and LIM/OH/NOₓ SOA (right panels) conditions. The yellow region indicates the time during which the light was on for photooxidation. The purple region indicates the time during which 200 ppb of ammonia was added to the chamber. The $C_xH_yN_z^+$ family of ToF-AMS fragments is plotted in black in the top panels. The NH family of fragments is plotted in green in the middle panels. The NO family of fragments is plotted in red in the bottom panels. Reproduced with permission from the Ph.D. dissertation by Mallory Hinks (70). Copyright 2017 under creative commons attribution license.

The $C_xH_yN_z^+$ ions also increased in the case of LIM/OH/NOₓ SOA (Figure 6), but some of these ions could conceivably be produced in the ToF-AMS electron impact ionizer because high-NOₓ SOA particles contained a large amount of ammonium nitrate (Figure 5). A similar increase in the $C_xH_yN_z^+$ ions in TOL/OH SOA and HEX/OH SOA exposed to ammonia could not be detected with sufficiently high signal-to-noise ratio, suggesting that different types of SOA have different reactivities towards ammonia.

The formation of NOC was additionally confirmed with off-line analysis of SOA particles collected on a filter by direct analysis in real time mass spectrometry (DART-MS) (70). The initial SOA compounds, before they were exposed to ammonia, consisted of only C, H, and O atoms, which typically appear at odd

nominal m/z in DART-MS (*71*). However, NOC with one nitrogen atom appeared at even m/z in DART-MS. From the observed increase in the relative intensity of the even m/z peaks compared to the odd m/z peaks, we could estimate the NOC molar fraction in the exposed SOA. The estimated fraction was the highest (up to 20%) in the LIM/O_3 SOA and dropped to 5% for TOL/OH SOA and HEX/OH SOA.

Modeling Reactive Uptake of Ammonia by SOA

The equilibria between ammonia and ammonium ion driven by reactions (R1-R3) are very important for predicting regional air quality and global climate effects of aerosols. These equilibria have been incorporated in all major air quality models. In contrast, only two studies (both done by our group) have examined the effect of the ammonia + SOA chemistry on air quality (*72*, *73*). While the ammonia + SOA → NOC reaction does not strongly affect the mass concentration of organic particulate compounds (e.g., see Figure 5), it can convert more basic ammonia (pK$_b$ ~ 5) into less basic NOC such as imines (pK$_b$ ~ 13) and pyrroles (pK$_b$ ~ 9). This may lead to a reduction in the amount of ammonium nitrate produced by reaction (R3), and therefore a reduction in the overall concentration of PM$_{2.5}$.

Furthermore, the particle pH can also be affected by shifting the relative amount of sulfate and bisulfate anions in the particle in reactions (R1-R2). Sulfuric acid has a low volatility such that it readily finds its way into particles, even in the absence of ammonia. This results in highly acidic particles when the ammonia concentration is low. As the concentration of ammonia increases, the sulfuric acid becomes more neutralized and the pH is increased. However, because of the buffering between gaseous ammonia and particle phase ammonium ion, the dependence of the particle acidity on the ammonia concentration is highly non-linear. As mentioned above, unrealistically high concentrations of ammonia are needed to achieve pH-neutral conditions in ambient particles (*10*, *11*).

Our modeling approach is illustrated in Figure 7. Since experimental information about the ammonia uptake by SOA particles is currently quite limited, we modeled this process in the simplest possible way as an irreversible conversion of ammonia into NOC on surfaces of SOA particles. The same reactive uptake coefficient, γ, for ammonia was assumed regardless of the SOA type, and no dependence of the uptake on particle acidity (*66*) or RH (*15*) noted in previous experiments was considered in our exploratory simulations. Furthermore, based on the experiments described above we assumed that no more than ~10% of SOA compounds can be converted into NOC. Even though this is arguably an oversimplified approach, it explores an important question: "How large must the reactive uptake coefficient for ammonia be for this chemistry to measurably affect air quality?"

Organic

NOC

γ

NH$_3$(g)

Inorganic

(NH$_4$)$_2$SO$_4$(s)

K_{eq}

H$_2$SO$_4$(g)

HNO$_3$(g)

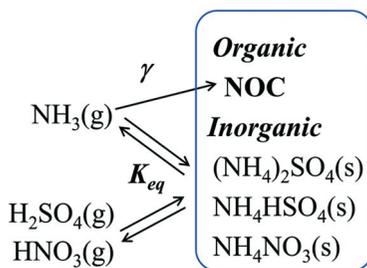NH$_4$HSO$_4$(s)

NH$_4$NO$_3$(s)

Figure 7. The simplest approach to modeling reactive uptake of ammonia by SOA. In addition to the equilibrium between ammonia and its inorganic salts in PM$_{2.5}$, an irreversible conversion of ammonia into NOC is added to the model, with its rate controlled by reactive uptake coefficient, γ. Since NOC is less basic than ammonia, formation of NOC reduces the amount of inorganic salts as well as affects the particle pH.

In our first study (73), we relied on the University of California, Irvine - California Institute of Technology (UCI-CIT) regional airshed model to investigate the potential impacts of this chemistry on the air quality in the SoCAB. The chemical mechanism used by the UCI-CIT model relies on the Caltech Atmospheric Chemical Mechanism (CACM) (74–76). The UCI-CIT model was previously used to simulate the effect of newly-discovered atmospheric chemistry on air quality in the SoCAB, for example in refs. (77–79). We added a surface reaction of ammonia with SOA particles to the base-case model and used uptake coefficients ranging from $\gamma = 10^{-5}$ to 10^{-2} to test the sensitivity of the model to this parameter. The largest effect on PM$_{2.5}$ was observed with $\gamma = 10^{-2}$, which resulted in a 15-40% reduction (depending on the time of day) in the domain-averaged ammonia concentration, and 2-12% reduction in the domain-averaged PM$_{2.5}$ concentration. In some locations, the reduction was considerably larger, as shown in Figure 8, particularly downwind from the large agricultural sources of ammonia in Chino, California. The predicted reduction in PM$_{2.5}$ concentrations was in excess of 10 μg/m^3 in the areas downwind from the major VOC and ammonia emissions, which is significant considering that the current U.S. National Ambient Air Quality Standards (NAAQS) for PM$_{2.5}$ concentrations is 35 μg/m^3 (24-hour average). The effect was still clearly observed in the model runs with $\gamma = 10^{-3}$, with the domain-averaged concentrations of ammonia and PM$_{2.5}$ dropping by 3-14% and 0.5-3%, respectively. For smaller values of the assumed γ values, the effect on ammonia and PM$_{2.5}$ concentrations was smaller, reducing to the level of the model noise when $\gamma = 10^{-5}$ was assumed. These model runs strongly suggested that if the uptake coefficient is indeed as large as reported by Liu et al. (2015), who reported the initial uptake coefficient of ~4×10^{-3} for α-pinene SOA and ~1×10^{-2} for xylene SOA (66), this could have a large effect on the distribution of both gaseous and particulate air pollutants in the SoCAB.
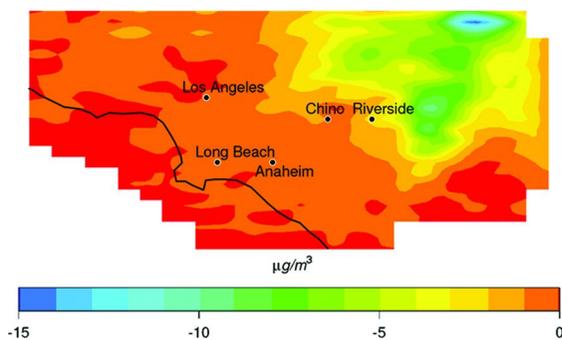
Figure 8. Difference from base case in 24-hour average of PM$_{2.5}$ when including ammonia uptake onto SOA using γ = 10^{-2}. The color bar is in the units of μg/m^3, with negative values indicating decreases in concentration with respect to the base case.

Inspired by the results of the regional airshed modeling with the UCI-CIT model, we extended the analysis to the continental United States (*72*). We added a first-order loss rate for ammonia onto SOA particles into the Community Multiscale Air Quality (CMAQ, version 5.2) model. The simulations covered the continental US in summer and winter periods. The initial CMAQ model simulations showed that predicted ammonia uptake with γ = 10^{-2} was unrealistically large, exceeding the assumed 10% limit for the NOC conversion from SOA compounds. Therefore, simulations performed with the CMAQ model used uptake coefficients ranging from 10^{-5} to 10^{-3} to provide more realistic results.

Figure 9 shows a sample result of the simulation (the maps for this figure were prepared by the NCAR Command Language (*80*)). Similar to the SoCAB study, the simulation with the largest γ = 10^{-3} predicted a reduction in the domain-averaged ammonia concentrations by about 30% in winter and 70% in summer. This reduction had two major effects. During the winter period, the model-predicted concentration of PM$_{2.5}$ dropped because of the smaller amount of ammonium nitrate particles formed, similar to the situation in the SoCAB simulations. However, in the summer period an increase in the amount SOA was predicted over the southeastern part of the US. This unanticipated result was driven by the reduction in the predicted particle pH (by up to two pH units), which led to an increase in the production of SOA by acid-catalyzed uptake of isoprene-derived epoxides (IEPOX). The IEPOX pathway was previously shown to improve SOA predictions in the southeastern US, and it is sensitive to the particle pH (*81*). We should note that the predicted drop in pH should be treated with caution and verified in future simulations as more accurate predictions of pH in aerosol particles become available. For example, it has been shown that particle pH is not especially sensitive to ammonia and particles in the southeastern United States remain acidic even when sulfate concentration drops and ammonia concentration increases (*11*).
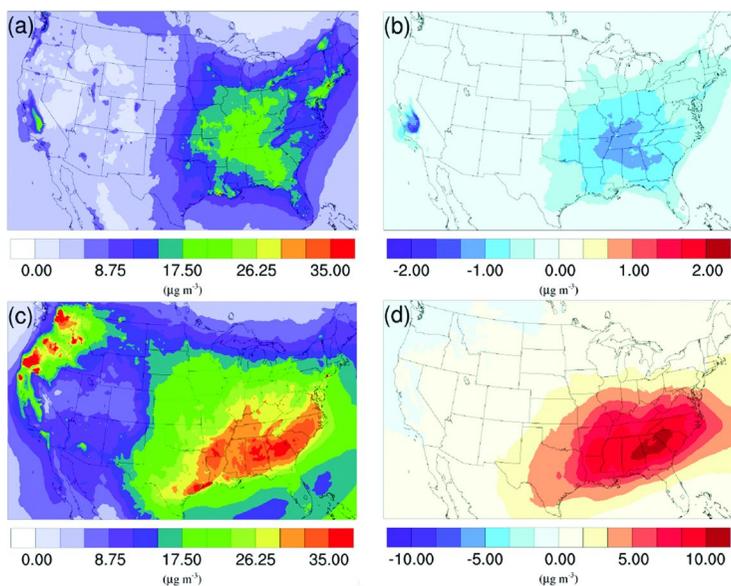
Figure 9. Spatial distribution of time-averaged PM$_{2.5}$ concentrations in the base case for (a) winter, and (c) summer. Spatial distribution of the difference in time-averaged PM$_{2.5}$ concentrations between the $\gamma = 10^{-3}$ case and the base case for (b) winter, and (d) summer. Positive values represent increases in concentration with respect to the base case, and negative values represent decreases in concentration with respect to the base case. Concentrations are expressed in units of µg/m^3. The figure is reproduced with permission from ref. (72). Copyright 2018 under creative commons attribution license.

Summary and Future Directions

The combination of experimental and modeling results described in this chapter show that it is critical to better understand the chemical processes involved in reactive uptake of ammonia by SOA particles. The predicted effects of these processes on air quality are substantial, and they can further increase in the future as POA concentrations decline due to control measures. The planet's population is expected to grow, with a steadily increasing demand for crop and cattle production. The concentration of ammonia will increase in parallel to the population growth and expanding agriculture. United Nations' Food and Agriculture Organization predicts that the annual ammonia emissions from livestock will increase by 60% by 2030 relative to the 1999 levels, with the largest increase occurring in the developing countries (82). The increased emissions of ammonia from livestock operations will be aided by warmer temperatures resulting from the changing climate because volatilization of ammonia is exponentially sensitive to temperature (83–85). For example, the anticipated increase in surface temperature predicted by an ensemble of seven different climate models could increase ammonia emissions in Europe by up to 40% by the end of the 21st century (86). The emissions of volatile organic compounds,

which act as SOA precursors, also increase steeply with temperature (*87*). The simultaneous rise in both ammonia and SOA concentrations will increase the relative importance of the reactive uptake of ammonia by SOA particles.

We have just scratched the surface with respect to understanding the mechanism of the ammonia + SOA chemistry. Considerable experimental and modeling research is needed before these reactions can be incorporated into all air quality models. There is a need to develop more accurate ammonia emission inventories and to increase the frequency and accuracy of ammonia field measurements so that future models can be tested against observations. The effects of the particle phase state and acidity on the rate of ammonia uptake needs to be explored in more detail. The reversibility of the reactive uptake of ammonia by SOA particles, and the chemical stability of the resulting NOC with respect to hydrolysis, photolysis, and oxidation need to be better understood. The basicity of NOC produced in the ammonia + SOA reactions needs to be better constrained. In our modeling studies we made a first assumption that these NOC cannot form salts with inorganic acids, but some of these NOC were in fact detected as nitrogen-containing organic salts (*56*). Finally, the effect of ammonia on $PM_{2.5}$ needs to be directly tested in cleverly designed field campaigns. In summary, we can anticipate a number of new targeted laboratory experiments, field measurements, and air quality modeling studies on this rapidly developing topic in the coming years. This is an urgent area of research because ammonia emissions are already on the rise while our understanding of ammonia chemistry in the atmosphere remains woefully inadequate.

Acknowledgments

References

1. Schlesinger, W. H.; Hartley, A. E. A global budget for atmospheric NH_3. *Biogeochemistry* **1992**, *15*, 191–211.
2. Dentener, F. J.; Crutzen, P. J. A 3-dimensional model of the global ammonia cycle. *J. Atmos. Chem.* **1994**, *19*, 331–369.
3. Bouwman, A. F.; Lee, D. S.; Asman, W. A. H.; Dentener, F. J.; VanderHoek, K. W.; Olivier, J. G. J. A global high-resolution emission inventory for ammonia. *Global Biogeochem. Cycles* **1997**, *11*, 561–587.
4. Clarisse, L.; Clerbaux, C.; Dentener, F.; Hurtmans, D.; Coheur, P. F. Global ammonia distribution derived from infrared satellite observations. *Nat. Geosci.* **2009**, *2*, 479–483.

5. Nowak, J. B.; Neuman, J. A.; Bahreini, R.; Middlebrook, A. M.; Holloway, J. S.; McKeen, S. A.; Parrish, D. D.; Ryerson, T. B.; Trainer, M. Ammonia sources in the California South Coast Air Basin and their impact on ammonium nitrate formation. *Geophys. Res. Lett.* **2012**, *39*, L07804.

6. Dentener, F.; Drevet, J.; Lamarque, J. F.; Bey, I.; Eickhout, B.; Fiore, A. M.; Hauglustaine, D.; Horowitz, L. W.; Krol, M.; Kulshrestha, U. C.; Lawrence, M.; Galy-Lacaux, C.; Rast, S.; Shindell, D.; Stevenson, D.; Van Noije, T.; Atherton, C.; Bell, N.; Bergman, D.; Butler, T.; Cofala, J.; Collins, B.; Doherty, R.; Ellingsen, K.; Galloway, J.; Gauss, M.; Montanaro, V.; Muller, J. F.; Pitari, G.; Rodriguez, J.; Sanderson, M.; Solmon, F.; Strahan, S.; Schultz, M.; Sudo, K.; Szopa, S.; Wild, O. Nitrogen and sulfur deposition on regional and global scales: A multimodel evaluation. *Global Biogeochem. Cycles* **2006**, *20*, GB4003.

7. Galloway, J. N.; Dentener, F. J.; Capone, D. G.; Boyer, E. W.; Howarth, R. W.; Seitzinger, S. P.; Asner, G. P.; Cleveland, C. C.; Green, P. A.; Holland, E. A.; Karl, D. M.; Michaels, A. F.; Porter, J. H.; Townsend, A. R.; Vorosmarty, C. J. Nitrogen cycles: past, present, and future. *Biogeochemistry* **2004**, *70*, 153–226.

8. Kim, E.; Turkiewicz, K.; Zulawnick, S. A.; Magliano, K. L. Sources of fine particles in the South Coast area, California. *Atmos. Environ.* **2010**, *44*, 3095–3100.

9. Chow, J. C.; Watson, J. G.; Fujita, E. M.; Lu, Z. Q.; Lawson, D. R.; Ashbaugh, L. L. emporal and spatial variations of $PM_{2.5}$ and PM_{10} aerosol in the Southern California air quality study. *Atmos. Environ.* **1994**, *28*, 2061–2080.

10. Guo, H. Y.; Weber, R. J.; Nenes, A. High levels of ammonia do not raise fine particle pH sufficiently to yield nitrogen oxide-dominated sulfate production. *Sci. Rep.* **2017**, *7*, 12109.

11. Weber, R. J.; Guo, H. Y.; Russell, A. G.; Nenes, A. High aerosol acidity despite declining atmospheric sulfate concentrations over the past 15 years. *Nat. Geosci.* **2016**, *9*, 282–286.

12. Laskin, A.; Laskin, J.; Nizkorodov, S. A. Chemistry of Atmospheric Brown Carbon. *Chem. Rev.* **2015**, *115*, 4335–4382.

13. Li, Y. J.; Liu, P. F.; Gong, Z. H.; Wang, Y.; Bateman, A. P.; Bergoend, C.; Bertram, A. K.; Martin, S. T. Chemical Reactivity and Liquid/Nonliquid States of Secondary Organic Material. *Environ. Sci. Technol.* **2015**, *49*, 13264–13274.

14. Bell, D. M.; Imre, D.; Martin, S. T.; Zelenyuk, A. The properties and behavior of alpha-pinene secondary organic aerosol particles exposed to ammonia under dry conditions. *Phys. Chem. Chem. Phys.* **2017**, *19*, 6497–6507.

15. Liu, P.; Li, Y. J.; Wang, Y.; Bateman, A. P.; Zhang, Y.; Gong, Z.; Bertram, A. K.; Martin, S. T. Highly Viscous States Affect the Browning of Atmospheric Organic Particulate Matter. *ACS Cent. Sci.* **2018**, *4*, 207–215.

16. Mang, S. A.; Henricksen, D. K.; Bateman, A. P.; Andersen, M. P. S.; Blake, D. R.; Nizkorodov, S. A. Contribution of carbonyl photochemistry to

aging of atmospheric secondary organic aerosol. *J. Phys. Chem. A* **2008**, *112*, 8337–8344.

17. Bones, D. L.; Henricksen, D. K.; Mang, S. A.; Gonsior, M.; Bateman, A. P.; Nguyen, T. B.; Cooper, W. J.; Nizkorodov, S. A. Appearance of strong absorbers and fluorophores in limonene-O_3 secondary organic aerosol due to NH_4^+-mediated chemical aging over long time scales. *J. Geophys. Res. D* **2010**, *115*, D05203.

18. Updyke, K. M.; Nguyen, T. B.; Nizkorodov, S. A. Formation of brown carbon via reactions of ammonia with secondary organic aerosols from biogenic and anthropogenic precursors. *Atmos. Environ.* **2012**, *63*, 22–31.

19. Aiona, P. K.; Lee, H. J.; Lin, P.; Heller, F.; Laskin, A.; Laskin, J.; Nizkorodov, S. A. A Role for 2-Methyl Pyrrole in the Browning of 4-Oxopentanal and Limonene Secondary Organic Aerosol. *Environ. Sci. Technol.* **2017**, *51*, 11048–11056.

20. Laskin, J.; Laskin, A.; Nizkorodov, S. A.; Roach, P.; Eckert, P.; Gilles, M. K.; Wang, B.; Lee, H. J.; Hu, Q. Molecular Selectivity of Brown Carbon Chromophores. *Environ. Sci. Technol.* **2014**, *48*, 12047–12055.

21. Nguyen, T. B.; Laskin, A.; Laskin, J.; Nizkorodov, S. A. Brown carbon formation from ketoaldehydes of biogenic monoterpenes. *Faraday Discuss.* **2013**, *165*, 473–494.

22. Nguyen, T. B.; Lee, P. B.; Updyke, K. M.; Bones, D. L.; Laskin, J.; Laskin, A.; Nizkorodov, S. A. Formation of nitrogen- and sulfur-containing light-absorbing compounds accelerated by evaporation of water from secondary organic aerosols. *J. Geophys. Res. D* **2012**, *117*, D01207.

23. Laskin, J.; Laskin, A.; Roach, P. J.; Slysz, G. W.; Anderson, G. A.; Nizkorodov, S. A.; Bones, D. L.; Nguyen, L. Q. High-Resolution Desorption Electrospray Ionization Mass Spectrometry for Chemical Characterization of Organic Aerosols. *Anal. Chem.* **2010**, *82*, 2048–2058.

24. De Haan, D. O.; Tolbert, M. A.; Jimenez, J. L. Atmospheric condensed-phase reactions of glyoxal with methylamine. *Geophys. Res. Lett.* **2009**, *36*, L11819.

25. Galloway, M. M.; Chhabra, P. S.; Chan, A. W. H.; Surratt, J. D.; Flagan, R. C.; Seinfeld, J. H.; Keutsch, F. N. Glyoxal uptake on ammonium sulphate seed aerosol: reaction products and reversibility of uptake under dark and irradiated conditions. *Atmos. Chem. Phys.* **2009**, *9*, 3331–3345.

26. Shapiro, E. L.; Szprengiel, J.; Sareen, N.; Jen, C. N.; Giordano, M. R.; McNeill, V. F. Light-absorbing secondary organic material formed by glyoxal in aqueous aerosol mimics. *Atmos. Chem. Phys.* **2009**, *9*, 2289–2300.

27. Noziere, B.; Dziedzic, P.; Cordova, A. Inorganic ammonium salts and carbonate salts are efficient catalysts for aldol condensation in atmospheric aerosols. *Phys. Chem. Chem. Phys.* **2010**, *12*, 3864–3872.

28. Sareen, N.; Schwier, A. N.; Shapiro, E. L.; Mitroo, D.; McNeill, V. F. Secondary organic material formed by methylglyoxal in aqueous aerosol mimics. *Atmos. Chem. Phys.* **2010**, *10*, 997–1016.

29. Schwier, A. N.; Sareen, N.; Mitroo, D.; Shapiro, E. L.; McNeill, V. F. Glyoxal-Methylglyoxal Cross-Reactions in Secondary Organic Aerosol Formation. *Environ. Sci. Technol.* **2010**, *44*, 6174–6182.

30. Trainic, M.; Abo Riziq, A.; Lavi, A.; Flores, J. M.; Rudich, Y. The optical, physical and chemical properties of the products of glyoxal uptake on ammonium sulfate seed aerosols. *Atmos. Chem. Phys.* **2011**, *11*, 9697–9707.

31. Yu, G.; Bayer, A. R.; Galloway, M. M.; Korshavn, K. J.; Fry, C. G.; Keutsch, F. N. Glyoxal in aqueous ammonium sulfate solutions: products, kinetics and hydration effects. *Environ. Sci. Technol.* **2011**, *45*, 6336–6342.

32. Galloway, M. M.; Loza, C. L.; Chhabra, P. S.; Chan, A. W. H.; Yee, L. D.; Seinfeld, J. H.; Keutsch, F. N. Analysis of photochemical and dark glyoxal uptake: Implications for SOA formation. *Geophys. Res. Lett.* **2011**, *38*, L17811.

33. De Haan, D. O.; Hawkins, L. N.; Kononenko, J. A.; Turley, J. J.; Corrigan, A. L.; Tolbert, M. A.; Jimenez, J. L. Formation of Nitrogen-Containing Oligomers by Methylglyoxal and Amines in Simulated Evaporating Cloud Droplets. *Environ. Sci. Technol.* **2011**, *45*, 984–991.

34. Zarzana, K. J.; De Haan, D. O.; Freedman, M. A.; Hasenkopf, C. A.; Tolbert, M. A. Optical properties of the products of α-dicarbonyl and amine reactions in simulated cloud droplets. *Environ. Sci. Technol.* **2012**, *46*, 4845–4851.

35. Kampf, C. J.; Jakob, R.; Hoffmann, T. Identification and characterization of aging products in the glyoxal/ammonium sulfate system – implications for light-absorbing material in atmospheric aerosols. *Atmos. Chem. Phys.* **2012**, *12*, 6323–6333.

36. Sareen, N.; Moussa, S. G.; McNeill, V. F. Photochemical aging of light-absorbing secondary organic aerosol material. *J. Phys. Chem. A* **2013**, *117*, 2987–2996.

37. Hamilton, J. F.; Baeza-Romero, M. T.; Finessi, E.; Rickard, A. R.; Healy, R. M.; Peppe, S.; Adams, T. J.; Daniels, M. J. S.; Ball, S. M.; Goodall, I. C. A.; Monks, P. S.; Borras, E.; Munoz, A. Online and offline mass spectrometric study of the impact of oxidation and ageing on glyoxal chemistry and uptake onto ammonium sulfate aerosols. *Faraday Discuss.* **2013**, *165*, 447–472.

38. Sedehi, N.; Takano, H.; Blasic, V. A.; Sullivan, K. A.; De Haan, D. O. Temperature- and pH-dependent aqueous-phase kinetics of the reactions of glyoxal and methylglyoxal with atmospheric amines and ammonium sulfate. *Atmos. Environ.* **2013**, *77*, 656–663.

39. Lee, A. K. Y.; Zhao, R.; Li, R.; Liggio, J.; Li, S.-M.; Abbatt, J. P. D. Formation of Light Absorbing Organo-Nitrogen Species from Evaporation of Droplets Containing Glyoxal and Ammonium Sulfate. *Environ. Sci. Technol.* **2013**, *47*, 12819–12826.

40. Rossignol, S.; Aregahegn, K. Z.; Tinel, L.; Fine, L.; Noziere, B.; George, C. Glyoxal Induced Atmospheric Photosensitized Chemistry Leading to Organic Aerosol Growth. *Environ. Sci. Technol.* **2014**, *48*, 3218–3227.

41. Drozd, G. T.; McNeill, V. F. Organic matrix effects on the formation of light-absorbing compounds from α-dicarbonyls in aqueous salt solution. *Environ. Sci.: Processes Impacts* **2014**, *16*, 741–747.

42. Powelson, M. H.; Espelien, B. M.; Hawkins, L. N.; Galloway, M. M.; De Haan, D. O. Brown Carbon Formation by Aqueous-Phase Carbonyl

Compound Reactions with Amines and Ammonium Sulfate. *Environ. Sci. Technol.* **2014**, *48*, 985–993.

43. Hawkins, L. N.; Baril, M. J.; Sedehi, N.; Galloway, M. M.; De Haan, D. O.; Schill, G. P.; Tolbert, M. A. Formation of Semisolid, Oligomerized Aqueous SOA: Lab Simulations of Cloud Processing. *Environ. Sci. Technol.* **2014**, *48*, 2273–2280.

44. Lin, P.; Laskin, J.; Nizkorodov, S. A.; Laskin, A. Revealing Brown Carbon Chromophores Produced in Reactions of Methylglyoxal with Ammonium Sulfate. *Environ. Sci. Technol.* **2015**, *49*, 14257–14266.

45. Zhao, R.; Lee, A. K. Y.; Huang, L.; Li, X.; Yang, F.; Abbatt, J. P. D. Photochemical processing of aqueous atmospheric brown carbon. *Atmos. Chem. Phys.* **2015**, *15*, 6087–6100.

46. Maxut, A.; Noziere, B.; Fenet, B.; Mechakra, H. Formation mechanisms and yields of small imidazoles from reactions of glyoxal with NH_4^+ in water at neutral pH. *Phys. Chem. Chem. Phys.* **2015**, *17*, 20416–20424.

47. Tang, M.; Alexander, J. M.; Kwon, D.; Estillore, A. D.; Laskina, O.; Young, M. A.; Kleiber, P. D.; Grassian, V. H. Optical and Physicochemical Properties of Brown Carbon Aerosol: Light Scattering, FTIR Extinction Spectroscopy, and Hygroscopic Growth. *J. Phys. Chem. A* **2016**, *120*, 4155–4166.

48. Li, W. Y.; Li, X.; Jockusch, S.; Wang, H.; Xu, B. L.; Wu, Y. J.; Tsui, W. G.; Dai, H. L.; McNeill, V. F.; Rao, Y. Photoactivated Production of Secondary Organic Species from Isoprene in Aqueous Systems. *J. Phys. Chem. A* **2016**, *120*, 9042–9048.

49. Hawkins, L. N.; Lemire, A. N.; Galloway, M. M.; Corrigan, A. L.; Turley, J. J.; Espelien, B. M.; De Haan, D. O. Maillard Chemistry in Clouds and Aqueous Aerosol As a Source of Atmospheric Humic-Like Substances. *Environ. Sci. Technol.* **2016**, *50*, 7443–7452.

50. Wong, J. P. S.; Nenes, A.; Weber, R. J. Changes in Light Absorptivity of Molecular Weight Separated Brown Carbon Due to Photolytic Aging. *Environ. Sci. Technol.* **2017**, *51*, 8414–8421.

51. Aiona, P. K.; Lee, H. J.; Leslie, R.; Lin, P.; Laskin, A.; Laskin, J.; Nizkorodov, S. A. Photochemistry of Products of the Aqueous Reaction of Methylglyoxal with Ammonium Sulfate. *ACS Earth Space Chem.* **2017**, *1*, 522–532.

52. De Haan, D. O.; Hawkins, L. N.; Welsh, H. G.; Pednekar, R.; Casar, J. R.; Pennington, E. A.; de Loera, A.; Jimenez, N. G.; Symons, M. A.; Zauscher, M.; Pajunoja, A.; Caponi, L.; Cazaunau, M.; Formenti, P.; Gratien, A.; Pangui, E.; Doussin, J. F. Brown Carbon Production in Ammonium-or Amine-Containing Aerosol Particles by Reactive Uptake of Methylglyoxal and Photolytic Cloud Cycling. *Environ. Sci. Technol.* **2017**, *51*, 7458–7466.

53. Stangl, C. M.; Johnston, M. V. Aqueous Reaction of Dicarbonyls with Ammonia as a Potential Source of Organic Nitrogen in Airborne Nanoparticles. *J. Phys. Chem. A* **2017**, *121*, 3720–3727.

54. Ackendorf, J. M.; Ippolito, M. G.; Galloway, M. M. pH Dependence of the Imidazole-2-carboxaldehyde Hydration Equilibrium: Implications for

Atmospheric Light Absorbance. *Environ. Sci. Technol. Lett.* **2017**, *4*, 551–555.

55. Debus, H. Ueber die Einwirkung des Ammoniaks auf Glyoxal. *Justus Liebigs Ann. Chem.* **1858**, *107*, 199–208.

56. Wang, X.; Gao, S.; Yang, X.; Chen, H.; Chen, J.; Zhuang, G.; Surratt, J. D.; Chan, M. N.; Seinfeld, J. H. Evidence for high molecular weight nitrogen-containing organic salts in urban aerosols. *Environ. Sci. Technol.* **2010**, *44*, 4441–4446.

57. Teich, M.; van Pinxteren, D.; Kecorius, S.; Wang, Z.; Herrmann, H. First Quantification of Imidazoles in Ambient Aerosol Particles: Potential Photosensitizers, Brown Carbon Constituents, and Hazardous Components. *Environ. Sci. Technol.* **2016**, *50*, 1166–1173.

58. Aregahegn, K. Z.; Noziere, B.; George, C. Organic aerosol formation photo-enhanced by the formation of secondary photosensitizers in aerosols. *Faraday Discuss.* **2013**, *165*, 123–134.

59. Palacios, L. G.; Arroyo, P. C.; Aregahegn, K. Z.; Steimer, S. S.; Bartels-Rausch, T.; Noziere, B.; George, C.; Ammann, M.; Volkamer, R. Heterogeneous photochemistry of imidazole-2-carboxaldehyde: HO2 radical formation and aerosol growth. *Atmos. Chem. Phys.* **2016**, *16*, 11823–11836.

60. Tsui, W. G.; Rao, Y.; Dai, H. L.; McNeill, V. F. Modeling Photosensitized Secondary Organic Aerosol Formation in Laboratory and Ambient Aerosols. *Environ. Sci. Technol.* **2017**, *51*, 7496–7501.

61. Velisek, J.; Davidek, T.; Davidek, J.; Trska, P.; Kvasnicka, F.; Velcova, K. New imidazoles formed in nonenzymic browning reactions. *J. Food Sci.* **1989**, *54*, 1544–6.

62. Rizzi, G. P. Chemical structure of colored Maillard reaction products. *Food Rev. Int.* **1997**, *13*, 1–28.

63. Meade Susie, J.; Miller Antonia, G.; Gerrard Juliet, A. The role of dicarbonyl compounds in non-enzymatic crosslinking: a structure-activity study. *Bioorg. Med. Chem.* **2003**, *11*, 853–62.

64. Wang, Y.; Ho, C. T. Flavour chemistry of methylglyoxal and glyoxal. *Chem. Soc. Rev.* **2012**, *41*, 4140–4149.

65. Kampf, C. J.; Filippi, A.; Zuth, C.; Hoffmann, T.; Opatz, T. Secondary brown carbon formation via the dicarbonyl imine pathway: nitrogen heterocycle formation and synergistic effects. *Phys. Chem. Chem. Phys.* **2016**, *18*, 18353–18364.

66. Liu, Y.; Liggio, J.; Staebler, R.; Li, S. M. Reactive uptake of ammonia to secondary organic aerosols: kinetics of organonitrogen formation. *Atmos. Chem. Phys.* **2015**, *15*, 13569–13584.

67. Song, M. J.; Liu, P. F. F.; Hanna, S. J.; Zaveri, R. A.; Potter, K.; You, Y.; Martin, S. T.; Bertram, A. K. Relative humidity-dependent viscosity of secondary organic material from toluene photo-oxidation and possible implications for organic particulate matter over megacities. *Atmos. Chem. Phys.* **2016**, *16*, 8817–8830.

68. Koop, T.; Bookhold, J.; Shiraiwa, M.; Poschl, U. Glass transition and phase state of organic compounds: dependency on molecular properties and

implications for secondary organic aerosols in the atmosphere. *Phys. Chem. Chem. Phys.* **2011**, *13*, 19238–19255.

69. Ye, Q.; Robinson, E. S.; Ding, X.; Ye, P.; Sullivan, R. C.; Donahue, N. M. Mixing of secondary organic aerosols versus relative humidity. *Proc. Natl. Acad. Sci. U. S. A.* **2016**, *113*, 12649–12654.

70. Hinks, M. L. Effect of Environmental Conditions on Composition and Photochemistry of Secondary Organic Aerosols. Ph.D. Thesis, University of California, Irvine, Irvine, CA, May 2017.

71. Nah, T.; Chan, M.; Leone, S. R.; Wilson, K. R. Real Time in Situ Chemical Characterization of Submicrometer Organic Particles Using Direct Analysis in Real Time-Mass Spectrometry. *Anal. Chem.* **2013**, *85*, 2087–2095.

72. Zhu, S. P.; Horne, J. R.; Montoya-Aguilera, J.; Hinks, M. L.; Nizkorodov, S. A.; Dabdub, D. Modeling reactive ammonia uptake by secondary organic aerosol in CMAQ: application to the continental US. *Atmos. Chem. Phys.* **2018**, *18*, 3641–3657.

73. Horne, J. R.; Zhu, S. P.; Montoya-Aguilera, J.; Hinks, M. L.; Wingen, L. M.; Nizkorodov, S. A.; Dabdub, D. Reactive Uptake of Ammonia by Secondary Organic Aerosols: Implications for Air Quality. *Atmos. Environ.* **2018** submitted.

74. Griffin, R. J.; Dabdub, D.; Seinfeld, J. H. Secondary organic aerosol 1. Atmospheric chemical mechanism for production of molecular constituents. *J. Geophys. Res. D* **2002**, *107*, 4332.

75. Griffin, R. J.; Dabdub, D.; Kleeman, M. J.; Fraser, M. P.; Cass, G. R.; Seinfeld, J. H. Secondary organic aerosol 3. Urban/regional scale model of size- and composition-resolved aerosols. *J. Geophys. Res. D* **2002**, *107*, 4334.

76. Dawson, M. L.; Xu, J. L.; Griffin, R. J.; Dabdub, D. Development of aroCACM/MPMPO 1.0: a model to simulate secondary organic aerosol from aromatic precursors in regional models. *Geosci. Model Dev.* **2016**, *9*, 2143–2151.

77. Montoya-Aguilera, J.; Horne, J. R.; Hinks, M. L.; Fleming, L. T.; Perraud, V.; Lin, P.; Laskin, A.; Laskin, J.; Dabdub, D.; Nizkorodov, S. A. Secondary organic aerosol from atmospheric photooxidation of indole. *Atmos. Chem. Phys.* **2017**, *17*, 11605–11621.

78. Perraud, V.; Horne, J. R.; Martinez, A. S.; Kalinowski, J.; Meinardi, S.; Dawson, M. L.; Wingen, L. M.; Dabdub, D.; Blake, D. R.; Gerber, R. B.; Finlayson-Pitts, B. J. The future of airborne sulfur-containing particles in the absence of fossil fuel sulfur dioxide emissions. *Proc. Natl. Acad. Sci. U. S. A.* **2015**, *112*, 13514–13519.

79. Carreras-Sospedra, M.; Lunden, M. M.; Brouwer, J.; Singer, B. C.; Dabdub, D. Air quality impacts of liquefied natural gas in the South Coast Air Basin of California. *J. Natural Gas Sci. Eng.* **2014**, *21*, 680–690.

80. *The NCAR Command Language*, Version 6.4.0 [Software]; UCAR/NCAR/ CISL/TDD: Boulder, CO, 2017.

81. Pye, H. O. T.; Pinder, R. W.; Piletic, I. R.; Xie, Y.; Capps, S. L.; Lin, Y.-H.; Surratt, J. D.; Zhang, Z.; Gold, A.; Luecken, D. J.; Hutzell, W. T.; Jaoui, M.; Offenberg, J. H.; Kleindienst, T. E.; Lewandowski, M.; Edney, E. O. Epoxide

Pathways Improve Model Predictions of Isoprene Markers and Reveal Key Role of Acidity in Aerosol Formation. *Environ. Sci. Technol.* **2013**, *47*, 11056–11064.

82. Bruinsma, J. *World Agriculture: Towards 2015/2030 : an FAO Perspective*; Food and Agriculture Organization (FAO): London, UK, 2003; pp 1−432.

83. Zhang, G.; Strom, J. S.; Li, B.; Rom, H. B.; Morsing, S.; Dahl, P.; Wang, C. Emission of ammonia and other contaminant gases from naturally ventilated dairy cattle buildings. *Biosyst. Eng.* **2005**, *92*, 355–364.

84. Bleizgys, R.; Bagdoniene, I.; Balezentiene, L. Reduction of the Livestock Ammonia Emission under the Changing Temperature during the Initial Manure Nitrogen Biomineralization. *Sci. World J.* **2013**, *2013*, 825437.

85. Pereira, J.; Misselbrook, T. H.; Chadwick, D. R.; Coutinho, J.; Trindade, H. Effects of temperature and dairy cattle excreta characteristics on potential ammonia and greenhouse gas emissions from housing: A laboratory study. *Biosyst. Eng.* **2012**, *112*, 138–150.

86. Skjøth, C. A.; Geels, C. The effect of climate and climate change on ammonia emissions in Europe. *Atmos. Chem. Phys.* **2013**, *13*, 117–128.

87. Constable, J. V. H.; Guenther, A. B.; Schimel, D. S.; Monson, R. K. Modelling changes in VOC emission in response to climate change in the continental United States. *Glob. Change Biol.* **1999**, *5*, 791–806.